Nano Energy (2016) 22, 169–178

Available online at www.sciencedirect.com

ScienceDirect

journal homepage: www.elsevier.com/locate/nanoenergy

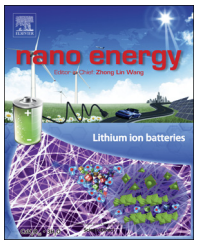

COMMUNICATION

Reversible Li-insertion in nanoscaffolds: A promising strategy to alter the hydrogen sorption properties of Li-based complex hydrides

Peter Ngene[a,*], Margriet H.W. Verkuijlen[b], Charlotte Barre[a], Arno P.M. Kentgens[b], Petra E. de Jongh[a,*]

[a]*Inorganic Chemistry and Catalysis, Debye Institute for Nanomaterials Science, Utrecht University, David de Wiedgebouw, Universiteitsweg 99, 3584 CG Utrecht, The Netherlands*
[b]*Institute for Molecules and Materials, Radboud University, Heyendaalseweg 135, 6525 AJ Nijmegen, The Netherlands*

Received 19 September 2015; received in revised form 14 January 2016; accepted 1 February 2016
Available online 8 February 2016

KEYWORDS
Hydrogen storage;
Complex hydrides;
Lithium insertion;
Thermodynamic destabilization;
Nanoconfinement;
Lithium borohydride

Abstract
Intercalation and de-intercalation of lithium into graphene layers is a well-established phenomenon in Li-ion battery technology. Here we show how this phenomenon can be exploited to destabilize, and alter the hydrogen sorption behaviour of Li-based metal hydrides ($LiBH_4$ and $LiAlH_4$), thereby achieving lower hydrogen release temperatures, high hydrogen sorption capacities and enhanced kinetics. Close contact between the hydride and carbon surface facilitates reversible intercalation of Li into graphene layers at moderate temperatures when nanoconfined in turbostratic carbon nanoscaffolds. This leads to the formation of intercalated Li (LiC_x, instead of LiH) during decomposition, resulting in the release of the full hydrogen content at moderate temperatures. For example, $LiBH_4$ nanoconfined in this graphitic carbon material decomposes into LiC_x+B and 18.5 wt% H_2 (instead of 13.8 wt% H_2 for macrocrystalline $LiBH_4$) at temperatures as low as 375 °C under Ar flow. Thermodynamic effects were also observed; the decomposition temperature at 1 bar H_2 atmosphere is lowered by ~150 °C compared to the macrocrystalline $LiBH_4$. These finding presents an interesting fundamental insight into interactions between nanoconfined metal hydrides and scaffold materials, and how such interactions can be exploited to generally improve the hydrogen sorption properties of metal hydrides.

*Corresponding authors.
E-mail addresses: P.Ngene@uu.nl (P. Ngene), P.E.dejongh@uu.nl (P.E. de Jongh).

http://dx.doi.org/10.1016/j.nanoen.2016.02.003
2211-2855/

Introduction

The ever increasing global demand for energy and rising concern about anthropogenic global warming is driving the transition towards energy sources that are sustainable and non-polluting. However the use of renewable energy generated from sources like solar, wind, wave, and geothermal will critically depend on efficient energy storage. Due to its high gravimetric energy density, hydrogen is considered an important energy vector for a sustainable future [1]. It can be converted efficiently in a polymer electrolyte membrane (PEM) fuel cell to produce electricity for automobile or stationary applications without producing any toxic or greenhouse gases. Hydrogen can also serve as an energy buffer for renewable energy sources, and thus minimise the problems associated with the intermittent nature of the energy from renewable sources such as solar and wind [2,3]. However the use of hydrogen especially for mobile applications is seriously constrained by its low volumetric energy density which results in the need for compaction [1,4,5]. Conventional hydrogen storage devices such as high-pressure gas containers are used, but limited by safety concerns and energy penalties associated with compressing the gas. Solid state hydrogen storage in light weight metal hydrides has gained considerable attention as an alternative approach due to its advantages in terms of safety and high hydrogen densities. Li-based complex hydrides like $LiBH_4$, $LiAlH_4$ and $LiNH_2$ are among the promising hydrogen storage compounds due to their high hydrogen content. For example, $LiBH_4$ contains 18.5 wt% H_2, making it one of the highly investigated complex hydrides for reversible hydrogen storage. When heated, it undergoes partial decomposition to LiH, B and H_2 according to Eq. (1).

$$2LiBH_4 \leftrightarrow 2LiH + 2B + 3H_2 \quad (1)$$

Unfortunately the compound is thermodynamically very stable, with a standard enthalpy of -67 kJ/(mol of H_2) for reaction (1), implying that an equilibrium pressure of 1 bar H_2 would require temperatures >400 °C. Practically, temperatures as high as 450 °C in Ar have been reported for the decomposition of bulk $LiBH_4$, while even harsher conditions (12 h at 600 °C and 155 bar H_2) are required for only partial rehydrogenation of the dehydrogenated materials [6,7]. These thermodynamical and kinetical limitations hamper the use of $LiBH_4$ for practical hydrogen storage. On the other, hand $LiAlH_4$ is metastable at room temperature therefore its decomposition is not readily reversible at moderate conditions.

Significant efforts have been made in the last decade to lower the enthalpy change for hydrogen release from $LiBH_4$ so that the equilibrium hydrogen release temperatures can be reduced to 100–150 °C which is required for combination with polymer electrolyte membrane (PEM) fuel cell applications. Mixing with other compounds is the main approach that has been intensely investigated. This is based on mixing $LiBH_4$ with other elements or compound which can either weaken the strong ionic bond between the Li^+ and $(BH_4)^{-1}$ [8–12] or result in the formation of more stable dehydrogenation products [13–16], and thereby decrease the enthalpy change for dehydrogenation. A notable one is a mixture of $LiBH_4$ and MgH_2 which forms MgB_2 (instead of B), and LiH upon dehydrogenation, and this reduces the enthalpy for the dehydrogenation reaction by 25 kJ/(mol of H_2) compared with pure $LiBH_4$ [14]. However the system still need the addition of TiCl as catalyst to increase the hydrogen sorption kinetics while substantial hydrogen release only occurs around 350 °C. Other systems based on reactant destabilization especially the double cation borohydrides [8–12] generally suffers from irreversibility due to phase segregation upon dehydrogenation.

Another approach that has been shown to be effective especially for improving hydrogen release kinetics and reversibility is nanoconfinement in carbon based scaffolds [2,17–19]. The improved release and uptake kinetics for nanoconfined $LiBH_4$ is attributed to the increased surface area to volume ratio at nanoscales, short solid-state diffusion distances (due to confinement of the dehydrogenated phases; B and LiH) and support effects. Although nanosizing is effective in improving hydrogen release kinetics and reversibility in $LiBH_4$, it does not mitigate the problem of high thermodynamic stability. Berube et al. [20,21] showed that at nanoscales, the contribution of the surface energy term becomes important to the total energy change upon decomposition of the metal hydride. If the surface energy of the metal hydride phase is larger than that of the metal, decreasing the size of the nanoparticles will generally lead to a lower relative stability of the hydride phase. This is the case for ionic or conventional metal hydrides like MgH_2 which show substantial decrease in stability when their sizes are reduced to dimensions between 2–5 nm, as the surface energy of the hydride is much higher than that of the resulting decomposition product (metallic Mg) [20–22]. However complex hydrides like $LiBH_4$ and $NaAlH_4$ possess much lower surface energies than their decomposition products. For example the surface energies of $LiBH_4$ and LiH are 0.12 J/m^2 and 0.44 J/m^2 respectively [23,24]. This implies that nanosizing of $LiBH_4$ will lead to effective stabilization of the hydride phase, hence higher equilibrium decomposition temperatures compared to the macrocrystalline samples, as already demonstrated for $NaAlH_4$ [24–28]. The significantly lower desorption temperatures reported for nanoconfined $LiBH_4$ can mostly be attributed to kinetic effects and irreversible reaction with scaffolds and/or impurities in the scaffolds to form oxides [29], carbides (B–C bonds [30] and LiC_2 [31]), titanates [32,33] and silicates [34,35].

In this work we exploits reversible Li insertion into graphitic carbon nanoscaffolds as a means to destabilize, and alter the decomposition pathway of $LiBH_4$, and thereby achieve low hydrogen release temperatures and high (de) hydrogenation kinetics. Electrochemical intercalation and de-intercalation of metallic Li into graphene layers is a well-established phenomenon in Li-ion battery technology. We show how this phenomenon can be exploited to generally alter the hydrogen sorption properties of Li-based complex hydrides. For $LiBH_4$ and $LiAlH_4$ incorporated into the pores of high purity graphitic carbon, the close contact between the compound and carbon surface facilitates reversible Li insertion into the graphene layers during (de)hydrogenation. This alters their dehydrogenation pathway resulting in full decomposition into the metal (B or Al) and intercalated Li (LiC_x, instead of LiH) at relatively low temperatures, while releasing the full hydrogen content of these

compounds. In addition, the equilibrium decomposition temperature (at 1 bar H_2 atmosphere) of $LiBH_4$ nanoconfined in this graphitic nanoscaffold is lowered by $\sim$150 °C compared to the macrocrystalline compound. We show clear evidence of this thermodynamical destabilization and altered decomposition pathway using hydrogen release measurements under H_2 pressure, X-ray diffraction and solid state NMR spectroscopy.

Experimental section

High surface area graphite (HSAG-500) from Timcal Switzerland, and carbon aerogels were used as the nanoporous carbon materials for the confinement of $LiBH_4$. The HSAG-500 has a pore volume of 0.66 cm^3/g, BET surface area 500 m^2/g, and a broad pore size distribution dominated by 2–3 nm pores. The carbon aerogels were synthesized through resorcinol-formaldehyde condensation catalyzed by sodium carbonate as described by Pekala et al. [36]. Prior to use, they were dried at 650 °C for 5 h under a mixture of 10% H_2/Ar flow to remove oxygen-containing groups and to stabilize some of the reactive sites [29,37].

$LiBH_4$ (Acros-organics, 95% pure) was incorporated into the dried carbon materials by melt infiltration as described earlier [35]. The required amounts of carbon and $LiBH_4$ were mixed and placed in a graphite sample holder and inserted into a stainless steel autoclave. An initial pressure of 50 bar H_2 was applied and the sample was heated at 3 °C min^{-1} to 295 °C and allowed to stay for 30 min at 295 °C at a final pressure of $\approx$100 bar H_2. The sample was then allowed to cool down to room temperature, and the hydrogen gas was released. All further sample handling and storage was under Ar atmosphere in a glove-box (contamination typically less than 0.1 ppm of O_2 and H_2O) to avoid contamination and oxidation. Nanoconfinement of $LiAlH_4$ (sigma Aldrich, 95% pure) was achieved by wetness impregnation using a solution containg 0.8 g $LiAlH_4$ in 1 ml of dried THF. To avoid contamination the impregnation was done in a nitrogen filled glove box and dried at 35 °C under dynamic vacuum for 24 h.

Structural characterization was performed using X-ray diffraction (XRD), nitrogen (N_2) physisorption and both ^{11}B and ^{7}Li solid-state Nuclear Magnetic Resonance (NMR) spectroscopy. All measurements were done in air tight sample holders. XRD patterns were obtained at room temperature from 18 to 75° 2θ with a Bruker-AXS D8 Advance X-ray diffractometer setup using $CoK\alpha_{1,2}$ radiation with a wavelength (λ) of 1.79026 Å. The microstructure of the samples was determined using a transmission electron microscope (TEM), FEI Tecnai 20 with a field emission gun, operated at 200 kV. The samples were deposited onto Holey carbon grids (200 mesh) inside the glove box and transferred to the microscope in an airtight sample holder. Typically, during the insertion of the sample holder into the microscope column, the sample was exposed to air for about 2–5 sec.

N_2-physisorption measurements were performed at −196 °C, using a Micromeritics Tristar 3000 apparatus. The pore size distributions of the samples were calculated from the desorption branch using BJH theory with the Harkins and Jura thickness equation. Solid-state NMR experiments were performed on a 600 MHz Varian spectrometer using a 2.5 mm HX MAS probe. The 2.5 mm MAS rotors were in filled in a glovebox under a dry N_2 atmosphere. ^{11}B and ^{7}Li single pulse excitation spectra were obtained using a short hard pulse of 0.20 μs at an effective rf-field strength of 140 kHz after taking pulse rise and decay times into account. Spectra were acquired without proton decoupling. A sample spinning speed of 15 kHz was applied. The ^{7}Li spectra were referenced with respect to an aqueous solution of LiCl (δ=0 ppm). The ^{11}B spectra were referenced using an aqueous solution of H_3BO_3 as secondary reference with a chemical shift of δ=19.6 ppm relative to $BF_3 \cdot OEt_2$ (δ=0 ppm). All NMR data processing was done using matNMR [38].

Hydrogen release from the samples was measured by temperature programmed desorption (TPD) using a Micromeritics AutoChem II 2920 apparatus. 60 to 100 mg of sample was heated at 5 °C/min from room temperature to 400–500 °C in 25 ml/min Ar (99.99% purity) flow with a dwell time of 25 min at the maximum temperature. The amount of hydrogen released was analysed using the peak editor program of the AutoChem II 2920 based on calibration with standard H_2/Ar gas mixture containing 0–5% H_2. Rehydrogenation of samples after H_2 desorption was performed in an autoclave at 50 bar H_2 and 325 °C for 3 h after which the amount of H_2 absorbed by the sample was determined by a second TPD run. Isothermal hydrogen desorption and absorption measurements were done using a fully automated manometric Sievert type apparatus (PCTPro-2000 Setaram, pressure measurement accuracy: 1%). Desorption measurements were performed on approximately 100 mg of the sample at 400 °C starting with an initial pressure of about 17 bar H_2 which was lowered to $\sim$0.2 bar at the beginning of the measurement and then increases gradually due to hydrogen release from the sample (final pressure $\sim$0.45 bar H_2). The dehydrogenated samples were evacuated for 1 h and subsequently, hydrogen uptake measurements were done by charging the dehydrogenated sample with an initial pressure of 27 bar H_2 at 330 °C. Gravimetric hydrogen capacity (uptake and release) and thermodynamic measurements were performed in a magnetic suspension balance from Rubotherm. About 100 mg of the sample was loaded in a graphitic cup (stainless steel for bulk $LiBH_4$) and inserted into a stainless steel sample holder. The sample was heated at 2–5 °C/min to 400 °C under 1.1 bar H_2 at a constant flow of 25 ml/min. The amount of hydrogen released was determined from the weight changes after having corrected for buoyancy effects.

Results and discussions

Confinement of $LiBH_4$ into nanoporous graphite

The high surface area graphite (HSAG) used in this study can contain about 30 wt% $LiBH_4$ in the pores, however we initially limited the loading to 15 wt% $LiBH_4$ to ensure that all the $LiBH_4$ was indeed incorporated into the nanopores. Figures 1 and S1 (supporting information) shows respectively the XRD pattern and transmission electron micrographs of the HSAG, its physical mixture with 15 wt% $LiBH_4$ (PM), and the nanoconfined $LiBH_4$. Figure 1 indicates that $LiBH_4$ lacks

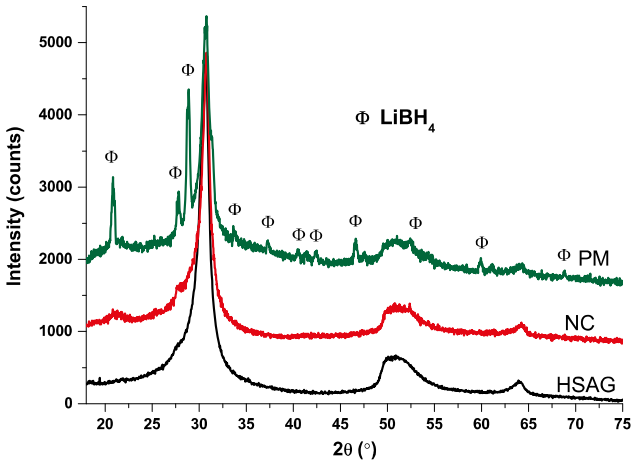

Figure 1 XRD patterns of the high surface area graphitic carbon support (HSAG), 15 wt% $LiBH_4$/C nanocomposite (NC) and a physical mixture of 15 wt% $LiBH_4$ and HSAG (PM).

long range/X-ray crystallinity after nanoconfinement, indicating that the vast majority of the $LiBH_4$ is incorporated in the pores of the scaffold [30,39-41]. Additional evidence for nanoconfinement is given by N_2 physisorption measurements which indicates that the total pore volume lost by the carbon is almost equal to the volume of $LiBH_4$ added to the composite (Figure S2 and Table S1 in supporting information), showing that the molten $LiBH_4$ does not reside outside of the scaffold but rather in the pores [35].

Thermodynamic effects in nanoconfined $LiBH_4$: H_2 Release under H_2 pressure

The equilibrium or thermodynamic decomposition of the samples was determined by temperature programmed hydrogen release measurements under H_2 pressure in a magnetic suspension balance. This method was adopted because manometric equilibrium isotherm measurements (PCT) for nanoconfined $LiBH_4$ are complicated due to the absence of a well-defined plateau pressure and the incomplete reversibility of $LiBH_4$. Figure 2 shows the hydrogen release profile from bulk and nanoconfined $LiBH_4$ at a constant pressure of 1.1 bar H_2, 25 ml/min H_2 flow, and at low heating rates (3 °C/min), thus approaching equilibrium measurements. As expected, no hydrogen was released from the bulk $LiBH_4$ upon heating to 400 °C. The National Institute of Standards (NIST) [42] reported −190.8 kJ/mol and −90.46 kJ/mol as the standard heats of formation (ΔH_f°) of $LiBH_4$ and LiH respectively, the entropy (S°) values for $LiBH_4$, LiH, B and H_2 are 75.88, 20.03, 5.90 and 130.7 J/(mol K) respectively. This would result in enthalpy ($\Delta_r H^\circ$) and entropy ($\Delta_r S^\circ$) change of 66.6 kJ/mol H_2 and 97.38 J/K mol H_2 for reaction (1) if the temperature dependence is neglected. This means a decomposition temperature of 410 °C for $LIBH_4$ at 1 bar H_2. Surprisingly the nanocomposite began to release hydrogen around 250 °C which is more than 150 °C lower than the expected decomposition temperature for bulk $LiBH_4$ at 1 bar H_2. About 10.5 wt% H_2/g $LiBH_4$ was released by the nanocomposite at 400 °C.

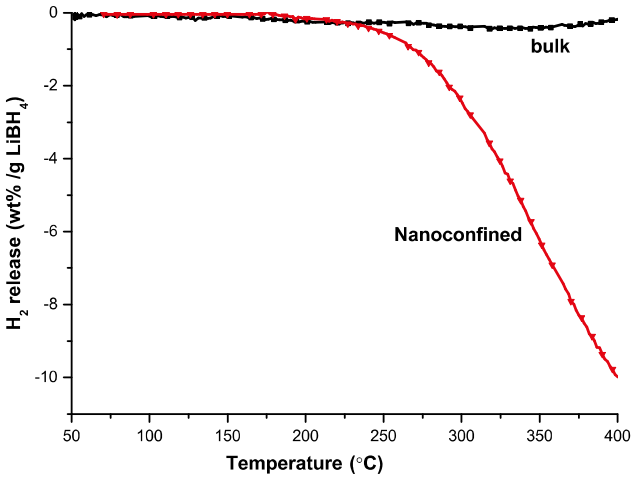

Figure 2 Hydrogen release from bulk and $LiBH_4$/C nanocomposites measured in Rubotherm suspension balance under 1.1 bar H_2 and 3 °C/min.

^{11}B and ^{7}Li NMR results (Figure 3) show that the chemical composition of the macrocrystalline $LiBH_4$ remained largely the same upon heating to 400 °C under 1.1 bar H_2 while the ^{11}B pattern of the nanocomposite shows additional peak around -5 ppm chemical shift which is most likely due to $Li_2B_{12}H_{12}$. Also, the peak of the ^{7}Li NMR pattern of the dehydrogenated nanocomposite is clearly different from that of the as-prepared nanocomposite, and the bulk $LiBH_4$ at room temperature and 400 °C. This observation confirms that the nanoconfined $LiBH_4$ has indeed undergone partial decomposition under these conditions. Note that the nanoscaffolds used here were subjected to extra purification treatment (by heating up to 650 °C under 10% H_2/N_2) so as to eliminate surface oxygen and/or carboxyl groups [29,43,44] that might influence the thermodynamics of hydrogen desorption from $LiBH_4$. $LiBH_4$ nanoparticles are predicted to be thermodynamically more stable than the macrocrystalline compound [27], and therefore should have higher equilibrium decomposition temperatures than the macrocrystalline $LiBH_4$. This is because although $LiBH_4$ nanoparticles are destabilized with respect to bulk, the reaction products are even more destabilized due to their relatively higher surface energy. However our results demonstrate that nanoconfinement of $LiBH_4$ in this graphitic scaffold led to its destabilization and/or a change in its decomposition pathway. This result is supported by a very recent result from computational studies which suggests that small clusters of $LiBH_4$ can be destabilized by the presence of graphitic carbon, forming intercalated Li and $Li_2B_{12}H_{12}$ upon decomposition (Eq. (2)) [45]. The authors showed that this route becomes unfavorable for larger $LiBH_4$ nanoparticles where dehydrogenation leads to the formation of LiH and B (Eq. (1)).

$$12LiBH_4 + 60C \leftrightarrow 10LiC_6 + Li_2B_{12}H_{12} + 18H_2 \quad (2)$$

Decomposition according to Eq. (2) will lead to a release of 13.8 wt% H_2, which is same as for decomposition according to Eq. (1). The release of about 10 wt% H_2 from our nanocomposite at 400 °C is because the $LiBH_4$ in the sample was only partially decomposed, as shown by ^{11}B NMR result which indicates the presence of $Li_2B_{12}H_{12}$ and undecomposed $LiBH_4$.

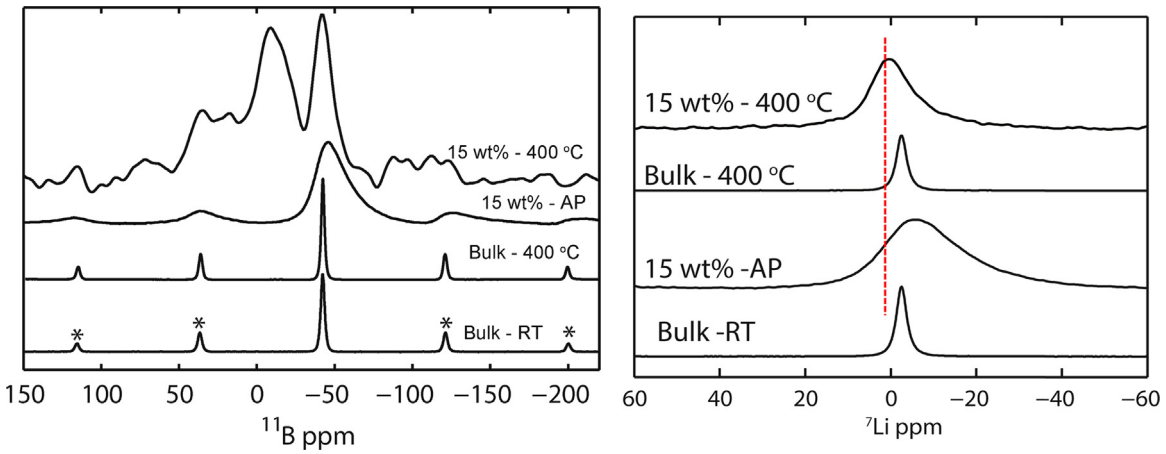

Figure 3 ^{11} B and ^{7}Li MAS NMR spectra of macrocrystalline $LiBH_4$ (Bulk) and the nanoconfined $LiBH_4$ in the as-prepared state (15 wt%-AP) at room temperature, and after heating to 400 °C under 1.1 bar H_2 (15 wt%-400 °C). * indicates the spinning sidebands.

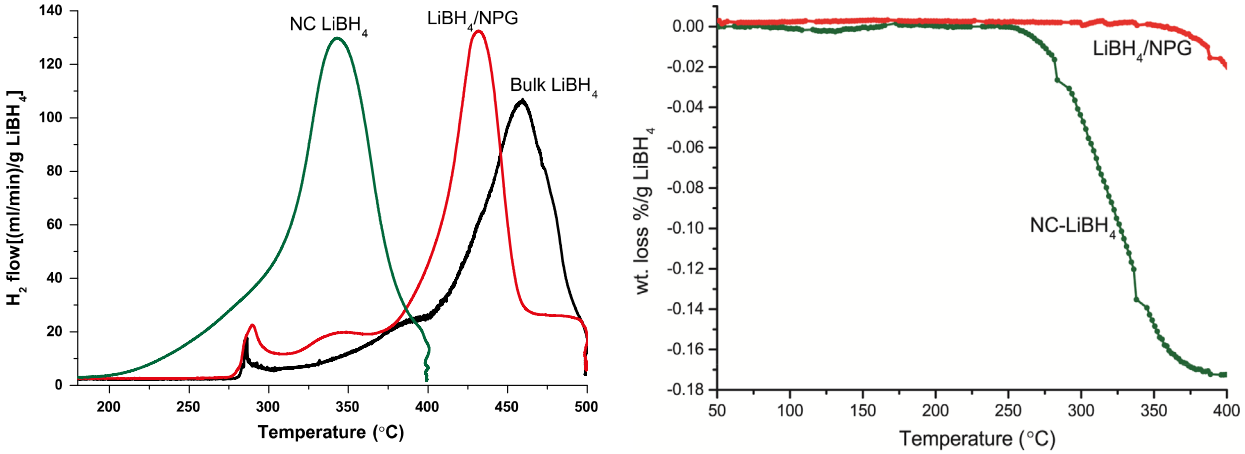

Figure 4 Hydrogen release behaviour of the samples while heating at 5 °C/min under 25 ml/min Ar flow. (a) Temperature programmed desorption (TPD) profiles for bulk $LiBH_4$, 15 wt% $LiBH_4$/non porous graphite (NPG) and the 15 wt% $LiBH_4$/C nanocomposite (b) Thermogravimetric hydrogen release profile of the samples (measured in Rubotherm suspension balance) showing that about 18 wt.% is released by the nanoconfined $LiBH_4$ upon heating to 400 °C in Ar.

We attribute this partial decomposition to the fraction of the $LiBH_4$ that are confined in very small nanopores, hence destabilized by the graphitic carbon, and decomposing according to Eq. (2) while the fraction confined in the bigger pores decomposes like the bulk compound under hydrogen atmosphere.

H_2 Desorption under Ar flow, and reversibility

Figure 4a shows the desorption profiles of the samples while heating under Ar. The bulk $LiBH_4$ and a composite of 15 wt% $LiBH_4$ and non-porous graphite ($LiBH_4$/NPG, used as reference) released hydrogen in multiple steps while the nanoconfined $LiBH_4$ released hydrogen in a single step, and at significantly lower temperatures than the other two samples. The significantly lower desorption temperature seen for the nanocomposites is in line with previous studies on nanoconfined $LiBH_4$; however an interesting observation stems from the amounts of hydrogen released by the samples. The bulk and $LiBH_4$/NPG released 11.4 and 13.4 wt% H_2 /g$LiBH_4$ respectively after heating to 500 °C and dwelling for 30 min. This corresponds to decomposition into LiH and B according to Eq. (1) which is the accepted decomposition pathway of $LiBH_4$, and should result in the release of 13.8 wt% H_2. Surprisingly the nanoconfined $LiBH_4$ released ~18.1 wt% H_2 after heating to 400 °C and dwelling for 30 min at this temperature. This is further confirmed by results from thermogravimetric hydrogen release measurements (Figure 4b), and mass spectrometry measurement (Figure S3) which shows that the mass lost by the sample is indeed due to hydrogen release. These observations strongly suggest that complete decomposition of $LiBH_4$ into Li, B and H_2 (Eq. (3)) is very likely in this sample, as this would lead to the release of 18.5 wt% H_2. This is remarkable because LiH is a very stable compound, and known to decompose at temperatures as high as 900 °C [46-48].

$$LiBH_4 \leftrightarrow Li + B + 2H_2 \quad (3)$$

The dehydrogenated nanocomposite also exhibited hydrogen uptake at mild conditions (at 325 °C, 50 bar H_2) while only a negligible amount of hydrogen was absorbed by the dehydrogenated bulk and $LiBH_4$/NPG samples (Figure 5).

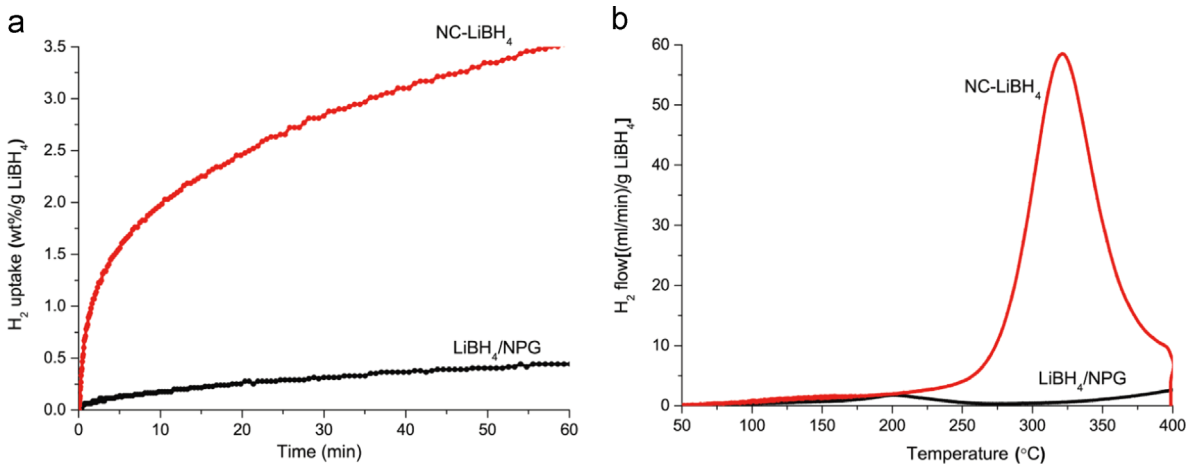

Figure 5 (a) Volumetric (Sievert) measurement showing hydrogen uptake (by the dehydrogenated samples) at 330 °C and initial pressure of ~27 bar H_2. (b) TPD profiles showing hydrogen release (5 °C/min, 25 ml/min Ar flow) from the rehydrogenated $LiBH_4$/NPG, and the nanoconfined $LiBH_4$.

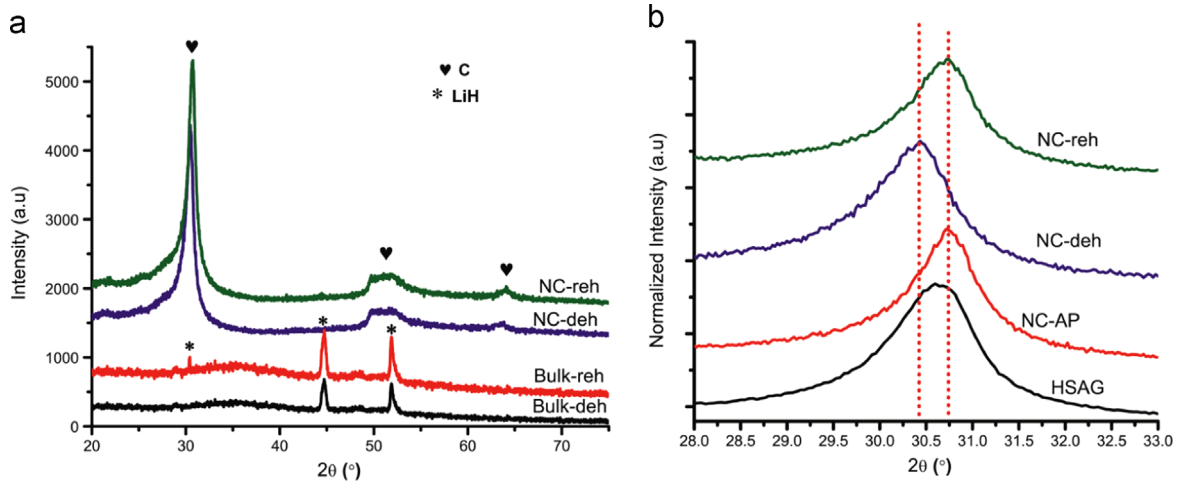

Figure 6 (a) XRD pattern of bulk and nanoconfined (NC) $LiBH_4$ after dehydrogenation (deh) and rehydrogenation (reh) in autoclave at 325 °C and 50 bar H_2 for 3 h. (b) XRD patterns showing a reversible shift in the C(002) diffraction peak of the nanoporous carbon (HSAG) after dehydrogenation and rehydrogenation of the nanoconfined $LiBH_4$.

Structural evolution during (de)hydrogenation

The micro-structural changes occurring in the samples during dehydrogenation and re-hydrogenation were further examined using XRD and NMR measurements. The XRD pattern of the dehydrogenated bulk $LiBH_4$ (Figure 6a) shows diffraction lines due to LiH and a broad peak between 30°-40° 2θ which is possibly due to amorphous B and/or $Li_2B_{12}H_{12}$ [48-50]. This shows that the macrocrystalline $LiBH_4$ indeed decomposes according to Eq. (1) (at 500 °C). No tangible change was observed after rehydrogenation of the desorbed sample, confirming that hydrogen release in this sample is not readily reversed under the conditions used here. For the nanocomposite, only diffraction lines due to the graphitic carbon were observed in the dehydrogenated and rehydrogenated samples.

Since reversibility was observed for the nanocomposite, the absence of $LiBH_4$ diffraction lines in the rehydrogenated sample indicates that the rehydrogenated $LiBH_4$ is amorphous or nano-crystalline, as is the case after melt infiltration. However a closer look at the carbon (002) diffraction peak of the nanocomposites (Figure 6b) reveals an interesting phenomenon. It can be seen that the position of this peak is similar for the pure scaffold and the as-prepared nanocomposite but after dehydrogenation the peak shifted from ~31.00° 2θ to 30.22° 2θ, and shifted back to its original position upon rehydrogenation. We assign this reversible peak shift to intercalation and de-intercalation of Li into the graphene layers of the scaffold material to form LiC_x [45,51-53]. For reversible Li intercalation into graphitic carbon materials, a maximum of one Li atom can be inserted per six graphite atoms to form LiC_6. The ratio of Li to carbon in the nanocomposite is ~1:10. This implies that theoretically it is possible for all the Li in the nanocomposites to intercalate into the graphene layers during dehydrogenation leading to full decomposition of the nanoconfined $LiBH_4$ into LiC_{10} and B, and thereby releasing all the hydrogen in the compound. This would explain why 18.1 wt% H_2 (very close

to the theoretical 18.5 wt% H_2) was released by this sample upon heating to 400 °C under Ar. This is the first report of full decomposition of $LiBH_4$ at such low temperatures.

Additional experiments show that the sample was already fully decomposed at 375 °C. Also the amount of hydrogen released by the nanocomposite decreased to 14.8 and 13.4 wt%H_2/$LiBH_4$ when the concentration of $LiBH_4$ in the nanocomposite was increased to 25 and 35 wt% respectively. This is explained by the fact that only a maximum of 90% and 62% of the Li in the 25 and 35 wt% nanocomposites respectively, can be intercalated into the graphene layers (to form LiC_6) while the rest will desorb as bulk $LiBH_4$. Similarly, the hydrogen release and uptake kinetics decrease slightly with increasing amount of $LiBH_4$ in the nanocomposites as shown in Figures S4 and S5. Another interesting observation is that in contrast to HSAG scaffold, a nanocomposite containing 15 wt% $LiBH_4$ confined in carbon aerogel with similar surface area (550 m^2/g,) and average pore size of 4 nm, released only 13.5 wt% H_2/g $LiBH_4$ under similar conditions, in accord with literature [17]. This is tentatively ascribed to the fact that intercalation of Li is not expected to occur in this non-graphitic carbon material especially at these relatively low desorption temperatures as the carbon structure determines how easily it is intercalated. The importance of nanoconfinement in facilitating this reversible Li intercalation is underscored by the fact that the reference sample (15 wt% $LiBH_4$ melted on non-porous graphite) released only 13.4 wt% H_2, indicating decomposition according to Eq. (1).

Another proof for the role of reversible Li-intercalation comes from solid state NMR measurements. Figure 7 shows ^{7}Li and ^{11}B MAS NMR pattern of the physically mixed sample (PM) and those of a 15 and 35 wt% $LiBH_4$ nanocomposites in the as-prepared, dehydrogenated and rehydrogenated states. It can be seen from both figures that the peak due to $LiBH_4$ (in the physically mixed sample) was clearly broadened after nanoconfinement. Such line broadening has been reported previously, and was ascribed to susceptibility effects due to the close contact between $LiBH_4$ and the conductive graphitic scaffolds [52,54,55].

The dehydrogenated macrocrystalline $LiBH_4$ has a ^{7}Li resonance around 0 ppm chemical shift which corresponds

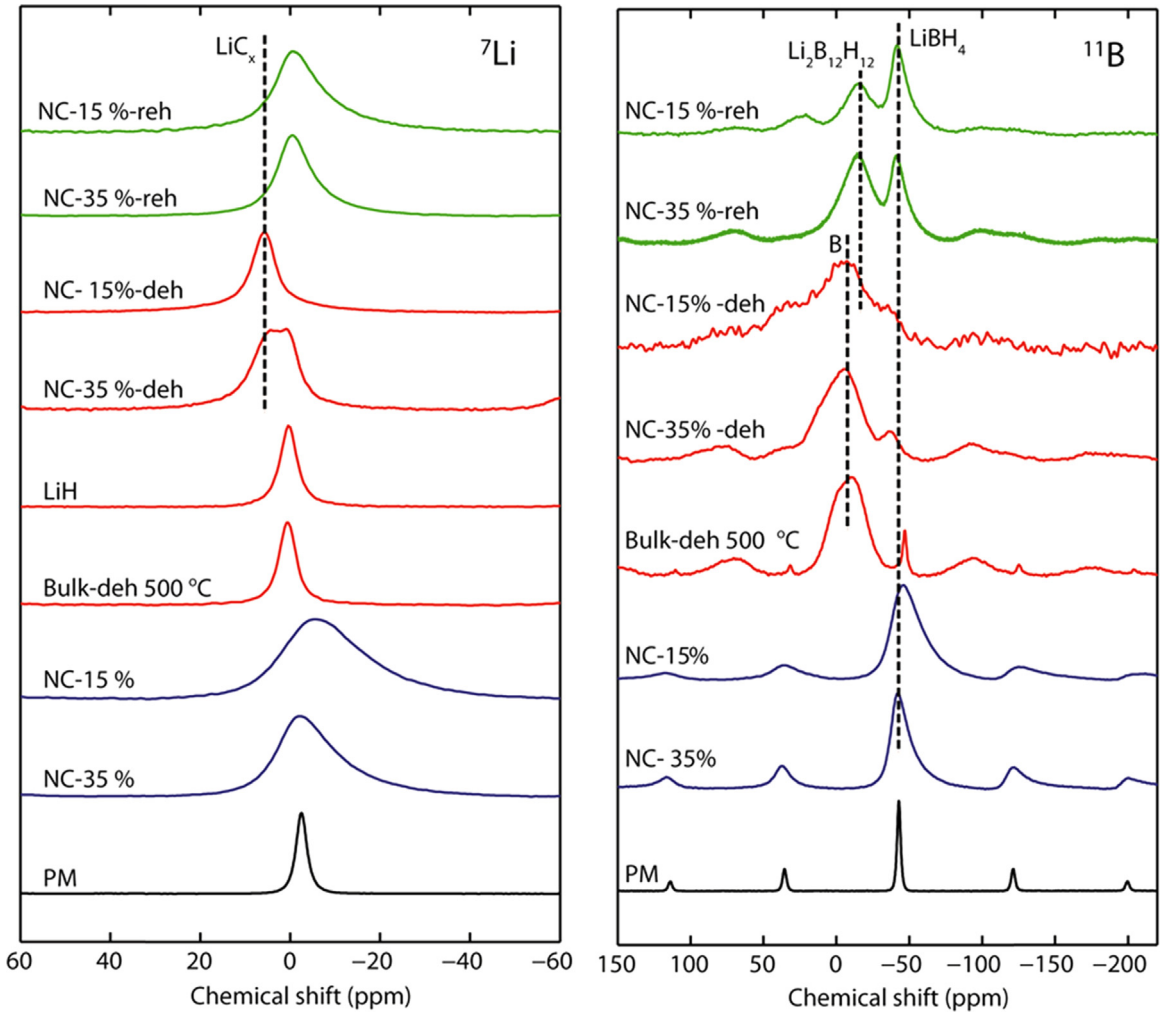

Figure 7 ^{7}Li and ^{11}B Magic angle spinning NMR pattern of a physical mixture (PM) of 15 wt% $LiBH_4$ and high surface area graphite, and nanocomposites (NC) containing 35 and 15 wt% $LiBH_4$ in the as prepared state, after dehydrogenation in Ar (deh) and rehydrogenation (reh) at 325 °C. Note that during desorption, the nanocomposites were heated to 400 °C while the bulk $LiBH_4$ was heated to 500 °C.

to the pattern of pure LiH, in agreement with the XRD results of this sample which show diffraction peaks due to LiH. The dehydrogenated 35 wt% $LiBH_4$ nanocomposite has a convoluted peak which is a combination of the resonance from LiH and a new resonance ~6 ppm chemical shift which can be attributed to LiC_x [56]. Interestingly, for the dehydrogenated 15 wt% $LiBH_4$ nanocomposite (NC-15%-deh) only the peak around 6 ppm chemical shift was observed, showing that only LiC_x is present in this sample. This result confirms that the Li phase in the dehydrogenated 15 wt% nanocomposite is not LiH but rather LiC_x while the 35 wt% nanocomposite contains a mixture of LiH and LiC_x. The XRD pattern of the dehydrogenated 35 wt% $LiBH_4$ nanocomposite also proves that LiH is present in this sample (Figure S6). After rehydrogenation, the peaks moved back to almost same position as the as-prepared nanocomposites. However the peak cannot be entirely attributed to $LiBH_4$ because $Li_2B_{12}H_{12}$ and LiH are also expected to be present in the rehydrogenated sample due to incomplete reversibility of the dehydrogenated components at the moderate conditions used here. The ^{11}B NMR pattern of the rehydrogenated nanocomposites confirms that $Li_2B_{12}H_{12}$ was indeed formed in these samples. Unfortunately $LiBH_4$, $Li_2B_{12}H_{12}$ and LiH have very close chemical shifts, and thus making it non-trivial to accurately determine the exact composition of the rehydrogenated Li phases from the NMR results.

These NMR results show that the decomposition pathway of $LiBH_4$ nanoconfined in high purity graphitic carbon material is clearly different from that of the macrocrystalline $LiBH_4$, and this is ascribed to the effects of reversible Li intercalation. A comparison of the NMR spectra of the samples dehydrogenated under Ar and H_2 (Figure S7) shows that the carrier gas has a significant influence on Li intercalation, and hence the decomposition pathway of the nanocomposites. Decomposition under Ar strongly facilitates intercalation (also at lower temperatures) than decomposition under hydrogen due to stabilization of $Li_2B_{12}H_{12}$ and LiH in the presence of hydrogen.

Effects of Li-insertion on H_2 release properties of nanoconfined $LiAlH_4$

The results discussed above clearly indicate that Li-intercalation is an effective strategy to destabilize or lower the hydrogen release temperatures of $LiBH_4$. To investigate the applicability of this to other Li-based complex hydrides, we studied the hydrogen release properties of $LiAlH_4$ nanoconfined in the graphitic nanoscaffold via wetness impregnation of $LiAlH_4$ solution in THF. Results from XRD and N_2 physisorption measurements showed that the $LiAlH_4$ was indeed confined in the carbon pores (Figures S8 and S9). Figure 8 shows that the $LiAlH_4$/HSAG nanocomposite (NC- HSAG) releases hydrogen in three distinct steps, which corresponds to the three decomposition steps in Eqs. (4)-(6), while the other two samples show only two hydrogen release steps within the same temperature.

The nanocomposite released about 10 wt% H_2 (per g $LiAlH_4$) while the non-confined samples released ~7 wt% H_2. XRD indicates that the C(002) diffraction peak decreased with about 0.3° (2θ) after dehydrogenation, while LiH diffraction lines are clearly absent (Figure S8). These

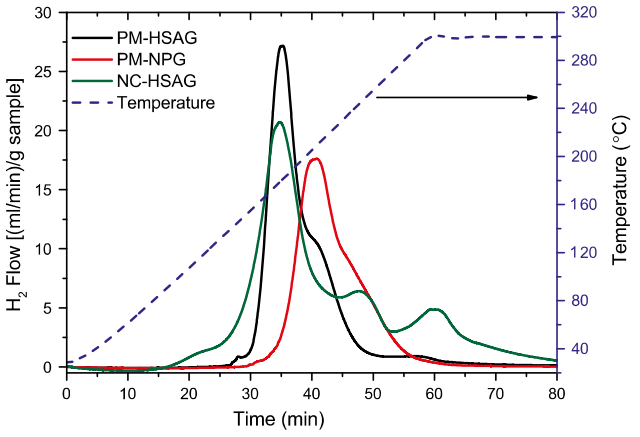

Figure 8 TPD profiles for $LiAlH_4$ physically mixed with high surface area turbostratic carbon (PM-HSAG), non-porous graphite (PM-NPG), and a nanocomposite of $LiAlH_4$and HSAG (NC-HSAG). All sample contains about 25 wt% $LiAlH_4$, desorption was at 5 °C/min under 25 ml/min Ar flow.

strongly suggest that confinement of $LiAlH_4$ in this turbostratic carbon material facilitates its full decomposition into LiC_x (instead of LiH), Al, and H_2 (Eqs. (4)-(6)) at this relatively low temperature (300 °C), while the macrocrystalline $LiAlH_4$ supported on non-porous graphite (PM-NPG) decomposes to Al, LiH and traces of undecomposed Li_3AlH_6 (Figure S9A) which are the expected decomposition products at this temperature [57-60]. Again, the importance of nanoconfinement in facilitating this Li-insertion is underscored by the fact that a physical mixture of $LiAlH_4$ and HSAG (PM-HSAG) decomposes mainly according to Eqs. (4) and (5). Successful confinement of $LiAlH_4$ in other carbon nanoscaffolds

$$3LiAlH_4 \rightarrow Li_3AlH_6 + 2Al + 3H_2 \quad (4)$$

$$Li_3AlH_6 \rightarrow 3LiH + Al + 3/2H_2 \quad (5)$$

$$3LiH + 16C \rightarrow 3LiC_6 + 3/2H_2 \quad (6)$$

has been reported [59,60], however this is the first report, as far as we are aware, of full decomposition of $LiAlH_4$ (into Li, Al, and H_2) at relatively low temperatures, which is due to Li intercalation in the graphitic carbon nanoscaffold. Although thermodynamical limitations still hinder reversible formation of $LiAlH_4$ from the dehydrogenation products, our results shows that that the decomposition pathway of the compound can indeed be altered by Li intercalation. Preliminary results show that the hydrogen and NH_3 release from $LiNH_2$ are also influenced by reversible Li intercalation, showing the potential of Li (de)-intercalation as a strategy to generally alter the hydrogen sorption properties of all Li-based metal hydrides.

The practical relevance of nanoconfinement is generally limited by the reduction in the effective hydrogen content of metal hydrides due to the added weight of the nanoscaffolds. Additionally, the use of certain scaffold materials can reduce the reversible capacity of metal hydrides due to irreversible reactions during (de)hydrogenation processes. Nevertheless this work demonstrates that we can fundamentally destabilize $LiBH_4$, and increase the hydrogen

sorption kinetics and capacity of nanoconfined Li-based complex hydrides by exploiting reversible interactions between graphitic carbon and Li in the nanocomposites. This shows that the hydrogen storage properties of nanoconfined metal hydrides can further be enhanced by choosing appropriate scaffold materials.

Conclusions

The results presented above show clearly that the combination of nanoconfinement and reversible Li-insertion is a good approach to alter the hydrogen sorption properties of Li-based complex hydride such as $LiBH_4$ and $LiAlH_4$. Nanoconfinement in high purity graphitic nanoscaffolds facilitates reversible Li intercalation into the graphene layer of the scaffolds during hydrogen sorption process. This alters the stability and/or decomposition pathway of the metal hydride, resulting in full decomposition at relatively low temperatures than would be expected for the macrocrystalline compounds or when nanoconfined in non-graphitic carbon scaffolds. Although the use of scaffolds reduces the effective hydrogen density of nanoconfined metal hydrides, this work offers new fundamental insights on how to use reversible interactions between scaffold materials and metal hydride to achieve lower equilibrium hydrogen release temperatures and higher hydrogen sorption capacities in nanoconfined metal hydrides.

Acknowledgment

This work was financially supported by NWO-Vidi Netherlands, Project Number 016.072.316. We thank M. van Zwienen, A. van der Eerden and V. Koot for their technical support, and Timcal Ltd. Switzerland for providing the high surface area graphite, The Netherlands Organisation for Scientific Research (NWO) is acknowledged for its support of the solid-state NMR facility for advanced materials research at Radboud University Nijmegen. Finally we thank Dr. Jan van Bentum of Radboud University, Nijmegen for his support regarding the NMR results.

Appendix A. Supplementary material

Supplementary data associated with this article can be found in the online version at http://dx.doi.org/10.1016/j.nanoen.2016.02.003.

References

[1] A. Züttel, A. Remhof, A. Borgschulte, O. Friedrichs, Phil. Trans. R. Soc. A 368 (2010) 3329–3342.
[2] P.E. de Jongh, P. Adelhelm, Chemsuschem 3 (2010) 1332–1348.
[3] E.C. Rönnebro, E.H. Majzoub, MRS Bull. 38 (2013) 452–458.
[4] L. Schlapbach, A. Züttel, Nature 414 (2001) 353–358.
[5] J. Yang, A. Sudik, C. Wolverton, D.J. Siegel, Chem. Soc. Rev. 39 (2010) 656–675.
[6] P. Mauron, F. Buchter, O. Friedrichs, A. Remhof, M. Bielmann, C.N. Zwicky, A. Zuttel, J. Phys. Chem. B 112 (2008) 906–910.
[7] A. Züttel, A. Borgschulte, S.-I. Orimo, Scripta Mater. 56 (2007) 823–828.
[8] H.W. Li, S. Orimo, Y. Nakamori, K. Miwa, N. Ohba, S. Towata, A. Züttel, J. Alloys Compd. 446–447 (2007) 315–318.
[9] H. Hagemann, M. Longhini, J.W. Kaminski, T.A. Wesolowski, R. Černy, N. Penin, M.H. Sørby, B.C. Hauback, G. Severa, C.M. Jensen, J. Phys. Chem. A 112 (2008) 7551–7555.
[10] C. Kim, S.J. Hwang, R.C. Bowman Jr, J.W. Reiter, J.A. Zan, J.G. Kulleck, H. Kabbour, E.H. Majzoub, V. Ozolins, J. Phys. Chem. C 113 (2009) 9956–9968.
[11] D. Ravnsbæk, Y. Filinchuk, Y. Cerenius, H.J. Jakobsen, F. Besenbacher, J. Skibsted, T.R. Jensen, Angew. Chem. Int. Ed. 48 (2009) 6659–6663.
[12] E.A. Nickels, M.O. Jones, W.I.F. David, S.R. Johnson, R.L. Lowton, M. Sommariva, P.P. Edwards, Angew. Chem. Int. Ed. 47 (2008) 2817–2819.
[13] J.J. Vajo, G.L. Olson, Scripta Mater. 56 (2007) 829–834.
[14] J.J. Vajo, S.L. Skeith, F. Mertens, J. Phys. Chem. B 109 (2005) 3719–3722.
[15] M. Aoki, K. Miwa, T. Noritake, G. Kitahara, Y. Nakamori, S. Orimo, S. Towata, Appl. Phys. A 80 (2005) 1409–1412.
[16] U. Bösenberg, S. Doppiu, L. Mosegaard, G. Barkhordarian, N. Eigen, A. Borgschulte, T.R. Jensen, Y. Cerenius, O. Gutfleisch, T. Klassen, M. Dornheim, R. Bormann, Acta Mater. 55 (2007) 3951–3958.
[17] A.F. Gross, J.J. Vajo, S.L. Van Atta, G.L. Olson, J. Phys. Chem. C 112 (2008) 5651–5657.
[18] T.K. Nielsen, F. Besenbacher, T.R. Jensen, Nanoscale 3 (2011) 2086–2098.
[19] P.E. de Jongh, M. Allendorf, J.J. Vajo, C. Zlotea, MRS Bull. 38 (2013) 488–494.
[20] V. Berube, G. Chen, M. Dresselhaus, Int. J. Hydrogen Energy 33 (2008) 4122–4131.
[21] V. Berube, G. Radtke, M. Dresselhaus, G. Chen, Int. J. Energy Res. 31 (2007) 637–663.
[22] R.W.P. Wagemans, J.H. Van Lenthe, P.E. de Jongh, A.J. van Dillen, K.P. de Jong, J. Am. Chem. Soc. 127 (2005) 16675–16680.
[23] S.J. Binnie, S.J. Nolan, N.D. Drummond, D. Alfè, N.L. Allan, F.R. Manby, M.J. Gillan, Phys. Rev. B 82 (2010) 165431.
[24] Q. Ge, J. Phys. Chem. A 108 (2004) 8682–8690.
[25] J. Gao, P. Adelhelm, M.H.W. Verkuijlen, C. Rongeat, M. Herrich, P.J.M. Van Bentum, O. Gutfleisch, A.P.M. Kentgens, K.P. De Jong, P.E. De Jongh, J. Phys. Chem. C 114 (2010) 4675–4682.
[26] W. Lohstroh, A. Roth, H. Hahn, M. Fichtner, ChemPhysChem 11 (2010) 789–792.
[27] E. Hazrati, G. Brocks, G.A. de Wijs, J. Phys. Chem. C 116 (2012) 18038–18047.
[28] P. Vajeeston, P. Ravindran, H. Fjellvåg, Nanotechnology 20 (2009) 275704.
[29] J. Gao, P. Ngene, M. Herrich, W. Xia, O. Gutfleisch, M. Muhler, K.P. de Jong, P.E. de Jongh, Int. J. Hydrogen Energy 39 (2014) 10175–10183.
[30] N. Brun, R. Janot, C. Sanchez, H. Deleuze, C. Gervais, M. Morcrette, R. Backov, Energy Environ. Sci. 3 (2010) 824–830.
[31] Y. Zhang, W.-S. Zhang, A.-Q. Wang, S. Li-Xian, M.-Q. Fan, H.-L. Chu, J.-C. Sun, T. Zhang, Int. J. Hydrogen Energy 32 (2007) 3976–3980.
[32] X.B. Yu, D.A. Grant, G.S. Walker, J. Phys. Chem. C 112 (2008) 11059–11062.
[33] L. Guo, L. Jiao, L. Li, Q. Wang, G. Liu, H. Du, Q. Wu, J. Du, J. Yang, C. Yan, Int. J. Hydrogen Energy 38 (2013) 162–168.
[34] L. Mosegaard, B. Moller, J.E. Jorgensen, Y. Filinchuk, Y. Cerenius, J.C. Hanson, E. Dimasi, F. Besenbacher, T.R. Jensen, J. Phys. Chem. C 112 (2008) 1299–1303.
[35] P. Ngene, P. Adelhelm, A.M. Beale, K.P. de Jong, P.E. de Jongh, J. Phys. Chem. C 114 (2010) 6163–6168.
[36] R.W. Pekala, J. Mater. Sci. 24 (1989) 3221–3227.
[37] J.A. Menéndez, J. Phillips, B. Xia, L.R. Radovic, Langmuir 12 (1996) 4404–4410.

[38] J.D. van Beek, J. Magn. Reson. 187 (2007) 19–26.
[39] Z.Z. Fang, P. Wang, T.E. Rufford, X.D. Kang, G.Q. Lu, H.M. Cheng, Acta Mater. 56 (2008) 6257–6263.
[40] X.F. Liu, D. Peaslee, C.Z. Jost, E.H. Majzoub, J. Phys. Chem. C 114 (2010) 14036–14041.
[41] P. Ngene, M. van Zwienen, P.E. de Jongh, Chem. Commun. 46 (2010) 8201–8203.
[42] CRC Handbook of Chemistry and Physics, 2010-2011;91st Edition.
[43] J.A. Menéndez, B. Xia, J. Phillips, L.R. Radovic, Langmuir 13 (1997) 3414–3421.
[44] C. Moreno-Castilla, M.V. López-Ramón, F. Carrasco-Marína, Carbon 38 (2000) 1995--2001.
[45] E. Hazrati, G. Brocks, G.A. de Wijs, J. Phys. Chem. C 118 (2014) 5102–5109.
[46] S.V. Alapati, J.K. Johnson, D.S. Sholl, J. Phys. Chem. C 111 (2007) 1584–1591.
[47] J.J. Vajo, F. Mertens, C.C. Ahn, R.C. Bowman, B. Fultz, J. Phys. Chem. B 108 (2004) 13977–13983.
[48] M.P. Pitt, M. Paskevicius, D.H. Brown, D.A. Sheppard, C.E. Buckley, J. Am. Chem. Soc. 135 (2013) 6930–6941.
[49] O. Friedrichs, A. Remhof, S.J. Hwang, A. Züttel, Chem. Mater. 22 (2010) 3265–3268.
[50] S.J. Hwang, R.C. Bowman, J.W. Reiter, J. Rijssenbeek, G.L. Soloveichik, J.C. Zhao, H. Kabbour, C.C. Ahn, J. Phys. Chem. C 112 (2008) 3164–3169.
[51] G. Maurin, C. Bousquet, F. Henn, P. Bernier, R. Almairac, B. Simon, Chem. Phys. Lett. 312 (1999) 14–18.
[52] P. Ngene, M.H.W. Verkuijlen, Q. Zheng, J. Kragten, P.J.M. van Bentum, J.H. Bitter, P.E. de Jongh, Faraday Discuss. 151 (2011) 47–58.
[53] X.Y. Song, K. Kinoshita, T.D. Tran, J. Electrochem. Soc. 143 (1996) L120-L123.
[54] M.H.W. Verkuijlen, P. Ngene, D.W. de Kort, C. Barrel̀, A. Nale, E.R.H. van Eck, P.J.M. van Bentum, P.E. de Jongh, A.P.M. Kentgens, J. Phys. Chem. C 116 (2012) 22169–22178.
[55] M.H.W. Verkuijlen, J.B. Gao, P. Adelhelm, P.J.N. van Bentum, P. E. de Jongh, A.P.M. Kentgens, J. Phys. Chem. C 114 (2010) 4683–4692.
[56] N. Imanishi, K. Kumai, H. Kokugan, Y. Takeda, O. Yamamoto, Solid State Ionics 107 (1998) 135–144.
[57] H.W. Langmi, G.S. McGrady, X. Liu, C.M. Jensen, J. Phys. Chem. C 114 (2010) 10666–10669.
[58] J.W. Wiench, V.P. Balema, V.K. Pecharsky, M. Pruski, J. Solid State Chem. 177 (2004) 648–653.
[59] M.A. Wahab, J.N. Beltramini, Int. J. Hydrogen Energy 39 (2014) 18280–18290.
[60] P. Plerdsranoy, R. Utke, Int. J. Hydrogen Energy 40 (2015) 7083–7092.

Peter Ngene received his PhD in 2012 in Inorganic Chemistry and Catalysis, at the Utrecht University, the Netherlands. He was a postdoc for 3 years in the Chemical engineering departments, Delft University of Technology. He currently works as an assistant professor in Utrecht University. His research focus is on inorganic functional materials for energy storage, energy conversion and heterogeneous catalysis, with a particular interest on metal hydride nanocomposite materials for rechargeable batteries and for reversible hydrogen storage applications.

Margriet H. W. Verkuijlen received her MSc degree in physics in 2005 and her PhD degree in solid-state nuclear magnetic resonance spectroscopy in 2011, both from the Radboud University (the Netherlands). From 2009–2013, she was a researcher at the "Solid-state NMR facility for advanced materials research" of the Radboud University. In 2013 she continued her career in industry and joined ASML Netherlands B.V. as defect metrology engineer.

Charlotte Barre is currently pursuing her Ph. D. in Physics and Chemistry of Materials in Pierre and Marie Curie University (Paris) under the supervision of Prof. Clement Sanchez. She received her engineer diploma in Materials for Transport and Energy from The Graduate School of Chemistry, Biology and Physics of Bordeaux in 2011.Her interests are the materials related to energy storage.

Arno Kentgens received his Ph.D. in Physical Chemistry from Radboud University Nijmegen in 1987. He was a staff scientist at the Philips Research Laboratories in Eindhoven (1987–1988). From 1988–2000 he was supervisor solid-state NMR of the Dutch National HF-NMR facility. In 2000 he was appointed full professor for physical chemistry at Radboud University Nijmegen. He also heads the solid-state NMR facility for advanced materials science. The focus of his research is the development of novel NMR methodologies which is combined with realistic applications in materials science. A particular emphasis in the study of functional materials is directed toward energy conversion and storage.

Petra de Jongh received her PhD in photoelectrochemistry in 1999, and worked 5 years as a senior scientist at Philips Research. Since 2004 she works at Utrecht University, where she is now full professor of Inorganic Nanomaterials. Her research focus is on nanostructured inorganic materials (typically nanoparticles in mesoporous supports), and gaining insight in the impact of particle size, confinement and pore structure on the functionality of these materials for applications in catalysis and energy conversion and storage.